

## X-ray emission from HESS J1731-347/SNR G353.6-0.7

W.W. Tian<sup>1</sup>, Z. Li<sup>2</sup>, D.A. Leahy<sup>1</sup>, J. Yang<sup>3</sup>, X.J. Yang<sup>4</sup>, R. Yamazaki<sup>5</sup>, D. Lu<sup>3</sup>

### ABSTRACT

We present new results of the HESS J1731-347/SNR G353.6-0.7 system from *XMM-Newton* and Suzaku X-ray observations, and Delinha CO observations. We discover extended hard X-rays coincident with the bright, extended TeV source HESS J1731-347 and the shell of the radio SNR. A bright X-ray compact source is also detected near the center of the SNR. We find that spatially-resolved X-ray spectra can generally be characterized by an absorbed power-law model, with photon indice of  $\sim 2$ , typical of non-thermal emission. The compact source, in contrast, shows a much softer spectrum (with a photon index of  $\sim 4.7$ ). We find no evidence of a radio counterpart or an extended X-ray morphology for this source, making it unlikely to be a pulsar wind nebular (PWN) or an accreting neutron star. CO observations toward the inner part of the HESS source reveal a bright cloud component at  $-20 \pm 4$  km s<sup>-1</sup>, which is likely located at the same distance of  $\sim 3.2$  kpc as the SNR. Based on the probable associations between the X-ray and  $\gamma$ -ray emissions and between the CO cloud and the SNR, we argue that the extended TeV emission originates from the interaction between the SNR shock and the adjacent CO clouds rather than from a PWN.

*Subject headings:* (ISM:) supernova remnants-X-rays: observations-radio continuum: galaxy-radio lines

---

<sup>1</sup>Department of Physics & Astronomy, University of Calgary, Calgary, Alberta T2N 1N4, Canada, wtian@ucalgary.ca

<sup>2</sup>Harvard-Smithsonian Center for Astrophysics, 60 Garden Street, Cambridge, MA 02138, zyli@head.cfa.harvard.edu

<sup>3</sup>Purple Mountain Observatory, CAS, Nanjing 210008, China

<sup>4</sup>Department of Physics, University of XiangTan, China

<sup>5</sup>Department of Physical Science, Hiroshima University, Higashi-Hiroshima 739-8526, Japan

## 1. Introduction

The High Energy Stereoscopic System (HESS), with its excellent sensitivity and spatial resolution in the standard of  $\gamma$ -ray astronomy, greatly stimulates studies of very high energy astrophysics in recent years. A multi-wavelength approach has proven to be robust in shedding light on the nature of TeV sources. Among well-identified radio/X-ray counterparts of about 30 Galactic TeV sources<sup>6</sup>, young shell-type SNRs and pulsar wind nebulae are thought to be two major  $\gamma$ -ray generators (Bamba et al. 2003; Katagiri et al. 2005; Aharonian et al. 2006; Uchiyama et al. 2007; Chang et al. 2008; Camilo et al. 2009). Other candidates have also been proposed as counterparts of some unidentified TeV sources, e.g., old SNRs (Yamazaki et al. 2006; Fang & Zhang 2008), hypernova and  $\gamma$ -ray burst remnants (Ioka & Meszaros 2009), giant molecular clouds (GMC, Butt et al. 2008), and young stellar clusters (Aharonian et al. 2007). Recently, the extended TeV source HESS J1731-347 is found to almost entirely overlap an old radio/X-ray SNR candidate G353.6-0.7 (Aharonian et al. 2008; Tian et al. 2008, hereafter T08). The association between HESS J1731-347 and G353.6-0.7, as suggested by T08, makes this system a favorable laboratory for studying the generation of  $\gamma$ -rays in evolved SNRs. T08 considered the case of hardonic particle acceleration in an SNR shock encountering a dense molecular cloud, based on the theoretical model of Yamazaki et al. (2006), but conclusion remained to be drawn due to limitation of the data explored in their paper, i.e., low counting statistics of the *ROSAT* observation and the lack of high-resolution <sup>12</sup>CO maps. In this *Letter*, we report new results obtained from *XMM-Newton* and *Suzaku* X-ray observations and CO spectral-line data from Delinha 13.7 m radio telescope, which favor Yamazaki et al.’s scenario.

## 2. X-ray and Radio Observations

### 2.1. *XMM-Newton* and *Suzaku* Data

HESS J1731-347 was observed by *XMM-Newton* on March 21, 2007 (ObsID 0405680201; PI: G. Puehlhofer), with a 25 ksec exposure. We reduced the data obtained from the European Photon Imaging Camera (EPIC), using the *XMM-Newton* Science Analysis System (SAS), version 8.0. We selected EPIC-MOS and EPIC-pn events with patterns 0-12 and 0-4, respectively. An examination of the light curve indicated that the observation was contaminated by background flares. Cleaning of the high particle background results in effective exposure of 15.9, 11.8 and 6.2 ks for the MOS1, MOS2 and pn detectors, respectively. More-

---

<sup>6</sup><http://tevcat.uchicago.edu/>, <http://www.mppmu.mpg.de/~rwagner/sources/>

over, the observation was also contaminated by straylight<sup>7</sup>, presumably from a bright source, 1RXS J173157.7-335007 (Voges et al. 1999), located at  $\sim 50'$  off axis to the north and outside the field of view (FoV). Consequently, a substantial portion of the upper (northern) FoV of the MOS1 and pn detectors was contaminated (contamination in the MOS2 FoV is apparently minimal) and thus masked out from subsequent analysis. We produced counts and exposure maps for the three detectors, in the 0.8-1.5, 1.5-2.2 and 2.2-7 keV bands. The low energy cutoff is justified by the relatively high foreground absorption near the Galactic plane. We then merged the counts and exposure maps, accounting for the difference in the effective area among the three detectors. We also produced corresponding background maps, using the Filter Wheel Closed data that characterizes the quiescent particle background.

HESS J1731-347 was observed by Suzaku on Feb. 23, 2007 (ObsID 401099010; PI: G. Puehlhofer), with both X-ray Imaging Spectrometers (XIS, Koyama et al. 2007) and Hard X-ray Detector (Takahashi et al. 2007). The net exposure time is about 33 ks. In this work, we focus on the XIS Front-Illuminated (FI) CCDs that have very high efficiency and low background especially around 5 keV. Since the XIS2 became inoperable since November 2002, only data from XIS0 and XIS3 are used here. We used cleaned version 2.0 data (reduction by HEADAS software version 6.5). The background spectra were extracted from the off-source region in the same observation. In order to increase the statistics, the spectra from XIS0 and XIS3 were jointly fitted for subsequent analysis.

## 2.2. CO Data

We observe the G353.6-0.7/HESS J1731-347 system by employing the 13.7 meter Delinha millimeter telescope at the Purple Mountain Observatory in March 2008. The telescope has an angular resolution of  $55''$  at the observing frequencies. Simultaneously the three J=1-0 CO isotopic lines (i.e.,  $^{12}\text{CO}$ ,  $^{13}\text{CO}$ , and  $^{18}\text{CO}$ ) were observed by using a cryogenic superconducting SIS receiver and a multi-line backend spectroscopic system (Zuo et al. 2004), but only the  $^{12}\text{CO}$  was bright enough for significant detection. The system provides a velocity coverage from  $V_{LSR} = -150$  to  $60 \text{ km s}^{-1}$  and velocity resolution of  $0.37 \text{ km}^{-1}$  in  $^{12}\text{CO}$ . Three target spots (see Fig.1b), each with a size of  $5' \times 5'$ , were selected over the G353.6-0.7 area, which includes the center position at the TeV  $\gamma$ -ray peak (S1:[RA=17:32:00, Dec=-34:42:00]), and the *ROSAT* X-ray peak sites (S2: [173220, -345400], S3:[173250, -344600]), respectively. These regions were mapped with a grid size of  $1' \times 1'$ . Each point was integrated up to 6 minutes, resulting an average rms noise level in the spectra to be 0.2-0.3 K. Spectral line

---

<sup>7</sup>[http://xmm.esac.esa.int/external/xmm\\_user\\_support/documentation/uhb/node23.html](http://xmm.esac.esa.int/external/xmm_user_support/documentation/uhb/node23.html)

data were processed by the CLASS package of GILDAS software developed by IRAM.

### 3. Results

#### 3.1. X-ray emission

##### 3.1.1. X-ray image

Fig. 1 shows the overall X-ray morphology revealed by *XMM-Newton*, along with the radio continuum emission of G353.6-0.7 (Fig. 1a) and the  $\gamma$ -ray emission of HESS J1731-347 (Fig. 1b). The radio SNR has a shell-like morphology and an extent of  $\sim 30'$  in diameter, largely overlapping the extended HESS source. On the eastern half of the SNR, X-ray emission coincident with the radio emission was detected in an early *ROSAT* observation (T08). This is confirmed by the present *XMM-Newton* observation, although the lower (southern) part of the radio shell falls outside the *XMM-Newton* FoV. It is also evident that X-ray emission is present along the western half of the radio shell, which was not detected in the *ROSAT* observation albeit its larger FoV. This can be understood, as the emission is detected only in the 2.2-7 keV band that is beyond the *ROSAT* energy coverage.

A number of X-ray substructures are revealed under the moderate spatial resolution of *XMM-Newton*. In particular, a prominent filament is present within the shell, passing through the brightest (inner) part of the HESS source (Fig. 1b) and partially coincident with radio continuum emission (Fig. 1a). With comparable widths of  $\sim 2'$ , the filament and the eastern X-ray shell together define a ring-like feature (enclosed by the two dotted circles in Fig. 1a; hereafter referred to as the ring), along which there are several bright knots (highlighted by the small ellipses in Fig. 1a). Several plumes are present northwest of the ring, where the radio shell apparently breaks. From their projected positions, it is not clear whether the plumes are the natural extent of the shell or the filament. Furthermore, there is a bright compact source centering at (R.A., Dec.) = ( $17^{\text{h}}32^{\text{m}}03^{\text{s}}$ ,  $-34^{\circ}45'18''$ ), showing no counterpart on the radio image. This source is named XMMS J173203-344518 hereafter.

The ring is not necessarily a coherent feature. Nevertheless, subsequent analysis is focused on the X-ray emission along the ring, as it occupies the central portion of the *XMM-Newton* FoV that not subject to the straylight contamination. Fig. 2 shows the azimuthal distribution of the X-ray emission along the ring. Individual peaks, e.g., at position angles of  $\sim 120^{\circ}$ ,  $190^{\circ}$  and  $230^{\circ}$ , arise from the bright knots (hereafter referred to as K1, K2 and K3). The ring appears harder on its western half (i.e., the filament, in angular range of  $0^{\circ}$ - $180^{\circ}$ ) than on its eastern half (i.e., the shell).

### 3.1.2. X-ray spectra

We extract spectra, based on the EPIC-pn data, from various regions along the ring, including the three knots, the eastern half of the ring (K2 and K3 excluded), and the western half of the ring (i.e., the filament, K1 excluded). As the SNR fills almost the entire FoV, an ideal selection of local background is not possible. We choose to adopt a background spectrum from a 2.5-radius concentric circle within the ring, where the intensity appears to be among the lowest values across the FoV. Given the high intensities along the ring, our background adoption is not expected to introduce significant bias to the spectral fit. An absorbed power-law model is found to be an acceptable characterization for almost all the spectra, resulting in absorption column densities of  $\sim 10^{22}$  cm $^{-2}$  and photon-indices of  $\sim 2$ , typical of non-thermal emission. The only exception is the spectrum of the eastern ring (i.e., the shell), for which the power-law fit is not satisfactory, with a steeper photon-index of  $\sim 3$  indicative a possible thermal component at low energies. There is marginal evidence for the presence of an Fe K line at  $\sim 6.4$  keV in the spectrum of K2, further suggesting that the X-ray shell is at least partially thermal. The northwest region outside the ring (Fig. 1a) can also be fitted by an power-law with the index of about 2.2, but subject to large uncertainty due to the limited counts. The fit results are summarized in Table 1. The summed 2-10 keV intrinsic fluxes, derived from the best-fit models, are  $\sim 3.7 \times 10^{-12}$  ergs s $^{-1}$  cm $^{-2}$  for the western ring (including K1) and  $\sim 2.7 \times 10^{-12}$  ergs s $^{-1}$  cm $^{-2}$  for the eastern ring (including K2 and K3), respectively.

We also extract spectra for XMMS J173203-344518 from both the EPIC-pn and *Suzaku* XIS data although *Suzaku* XIS has a spatial resolution of  $\sim 1.8$  arcmin lower than that of the *XMM-Newton*. An absorbed power-law model is found to be an acceptable fit for both spectra, giving a steep photon index of  $\sim 4.7$  for the pn spectrum and  $\sim 4.3$  for the jointly-fitted XIS spectra (see Table 1). However, The compact source spectrum from *Suzaku* is fitted by a thermal model (Mewe,  $\chi^2/d.o.f.=218/235$ ) better than by an absorbed power law model ( $\chi^2/d.o.f.=231/236$ ). This shows that its emission is likely thermal. We obtain the *Suzaku* image centered on the bright compact source compact source. The compact source seems brighter in *Suzaku* map than in *XMM-Newton* map, indicating possible time variability. We discuss the nature of this source in § 4.

## 3.2. CO spectra

The three CO spectra (S1: J173200-344200; S2: J173220-345400; S3: J173250-344600) all show several bright cloud components (Fig. 3). Given a near kinematic distance of  $\sim 3.2$  kpc for G353.6-0.7, as inferred from the highest HI absorption feature at a velocity of  $\sim$

$-20\pm 4$  km s $^{-1}$  (T08), these CO spectra reveal increasing H $_2$  column density ( $\sim 2, 3$  and  $6 \times 10^{21}$  cm $^{-2}$  for S2, S3 and S1, respectively; see discussion section) towards the Galactic plane. A bright cloud component at  $-20\pm 4$  km s $^{-1}$  appears in the direction of S1 (i.e. near the intensity peak of the HESS source). This cloud is likely in front of the SNR and extends to the nearby bright HII region G353.42-0.37 to produces the deep HI absorption feature at  $-20\pm 4$  km s $^{-1}$  seen in the HI absorption spectrum from G353.42-0.37. Therefore it is plausible that the extended CO cloud is associated with the remnant and locates at same distance of  $\sim 3.2$  kpc as the HII region.

## 4. Discussion and conclusion

### 4.1. Nature of XMMS J173203-344518

A number of Galactic TeV objects are suggested to be PWNe (Kargaltsev & Pavlov 2008; Gaensler & Slane 2006). In view of the proximity between XMMS J173203-344518 and the projected centers of HESS J1731-347, it is worth considering a PWN origin for the  $\gamma$ -ray emission. In § 3 we showed that the spectra of XMMS J173203-344518 can be characterized by a power-law model with a photon index of  $\sim 4.7$ , which is much steeper than the typical values of PWNe ( $\sim 1.5 - 2.1$ ; Li, Lu & Li 2008). Neither is this index reminiscent of background active galactic nuclei or Galactic X-ray binaries, whose spectra, when fitted with a power-law model, show typical photon-indices of  $\sim 1.5 - 2$ .

The source appears a few times brighter in the Suzaku observation than in the *XMM-Newton* observation. This X-ray variability implies the possibility of detecting a cataclysmic variable (CV, e.g., Pretorius & Knigge 2007). We have examined the intra-observation (tens of ks in duration) light curves of the source but found no evidence for a flux variation, although we note that CVs do show X-ray variability on longer timescales. XMMS J173203-344518 does not appear in the CVs catalog<sup>8</sup>. We have also searched available archive data in optical<sup>9</sup> and infrared<sup>10</sup> bands with a matching radius of 6 arcsec (approximately the PSF FWHM of *XMM-Newton*-EPIC) and found a possible near-infrared counterpart ([R.A.,Dec.]=[J17h32m03.21s-34d45m18.70s]) but no optical counterpart. The near-infrared counterpart is a 13.8 magnitude star and cataloged in GLIMPSE II 08 Source Catalog. To conclude, the facts that XMMS J173203-344518 shows 1) a soft spectrum, 2) no radio

---

<sup>8</sup>2006 version:<http://heasarc.nasa.gov/W3Browse/all/cvcat.html>

<sup>9</sup>Digitised Sky Survey: <http://stdatu.stsci.edu/dss/>

<sup>10</sup>2MASS, GLIMPS and IRAS from NASA/IPAC infrared science archive: <http://irsa.ipac.caltech.edu>

counterpart, and 3) no extended morphology, strongly argue against a possible PWN origin for the HESS source.

#### 4.2. X-ray and $\gamma$ -ray emission mechanism

Based on a statistics of 5 young SNRs, Bamba et al. (2005) suggested the typical photon index of  $\sim 2.1 - 3.7$  for non-thermal SNRs. It is interesting that the hard X-ray emission of the ring in the HESS J1731-347/SNR G353.6-0.7 has similar photon index of  $\sim 2.2$ . But the SNR is old due to its extended ( $\sim 30$  arcmin in diameter) and faint radio emission (T08) so it should have a different high-energy mechanism. Old SNRs have quite different characteristics for the expected broad-band energy spectrum of accelerated electrons and protons than young SNRs (Yamazaki et al 2006). As an SNR ages, the acceleration time increases, allowing higher maximum energy of accelerated particles. However the losses also increase with time. The net result is that the electron spectrum is loss-limited when the SNR is older than  $\sim 10^3$  yr, but the proton spectrum only becomes loss-limited when the SNR is older than  $\sim 10^5$  yr. Therefore, in an old SNR, the  $\gamma$ - and X-ray emissions are expected to be dominated respectively by decay of neutral pions and by synchrotron radiation of secondary electrons from charged pion decay. These pions all result from collisions of primary protons and the ISM. One diagnostic is the ratio of TeV to X-ray synchrotron fluxes. If the protons are accelerated at the shock running into a GMC, for example, the ratio should then be a  $\lesssim 10$ , consistent with the value obtained for HESS J1834-087 (Tian et al. 2007). In contrast, if the cloud is only illuminated by the particles, the predicted ratio should then be greater than 100, due to the lack of magnetic field enhancement which would occur in the shock case (hence greatly enhancing the X-ray synchrotron emission).

The 2-10 keV unabsorbed *XMM-Newton* flux from the ring is  $\approx 4.3 \times 10^{-12}$  ergs  $\text{cm}^{-2}$   $\text{s}^{-1}$ . The  $\gamma$ -ray flux is  $F_{\gamma(1-10\text{TeV})} \approx 1.7 \times 10^{-11}$  ergs  $\text{cm}^{-2}$   $\text{s}^{-1}$  in the 1-10 TeV band, so the ratio  $R = F_{\gamma}/F_X$  is  $\sim 4.0$ . However, if we consider all the X-ray flux, including the heavily absorbed western-shell, the ratio of R might reduce to  $\sim 2$ .

For an old SNR ( $\sim 10^4$  yrs for SNR G353.6-0.7), Yamazaki et al. (2006) 's model shows that the flux in the 1-10 TeV band is a few times higher than that in 2-10 keV band if the TeV emission is from pion-decays, the X-rays are from synchrotron emissions of secondary electron (in the case of a shocked GMC). Synchrotron emissions from secondary electrons are about 3 orders of magnitude higher than that from primary electrons. Thermal X-ray emission is not considered in this model. However, there is little thermal emissions coming from an old SNR interior

The new Fermi large Area Telescope survey released a strong  $\gamma$ -ray source table in the range of 100 MeV - 100 GeV (Abdo et al. 2009). There is no strong GeV source within HESS J1731-347. For a case that TeV  $\gamma$ -ray and X-ray emissions originate from a shocked GMC, the GeV emission flux is about 2 orders of magnitude lower than that TeV flux (Fig. 5 of Yamazaki et al. (2006)) which is much low comparing with other cases (Figs 2 - 6), consistent with the explanation above.

New CO observations support such an SNR scenario: an extended CO cloud at  $\sim 20$  km s $^{-1}$  is associated with the SNR. From the spectrum of S1, we estimate an approximate H $_2$  column density of  $\sim 4 \times 10^{21}$  cm $^{-2}$  within the cloud, taking X factor of  $\sim 2.5 \times 10^{20}$  cm $^{-2}$  K $^{-1}$  km $^{-1}$ s (Solomon & Barrett 1991). Assuming the molecular cloud completely covers the SNR (at least over the extended HESS source region), then it has a mass of  $M_{H_2} = N_{H_2} \Omega d^2 (2m_H / M_\odot) \approx 5 \times 10^4 M_\odot$ . This is a GMC. S1 is located at the peak area of TeV source, and has a higher local H $_2$  column density than S2 and S3. This is consistent with the model of a shocked GMC. The evidence of increasing column density from lower-latitude region to higher-latitude region of the SNR revealed by the CO spectra give a plausible reason on the X-rays distribution. The ROSAT X-ray image of SNR G353.6-0.7 in the soft band (0.1-2.4 keV) appears only within the lower-latitude half of the radio remnant where the  $N_H$  is less than  $10^{22}$  cm $^{-2}$  (e.g. S3 and S2) because absorption blocks soft X-rays but not hard X-rays from the upper half where the  $N_H$  is larger than  $10^{22}$  cm $^{-2}$ . From the viewing-angle of observers, this gives a physical image that the GMC covers the SNR, so the TeV emissions cover the X-ray and radio emission regions. The coincidence of the X-ray morphology with both the radio and TeV  $\gamma$ -ray morphologies suggests that they are physically associated.

WWT and LDA acknowledge support from the Natural Sciences and Engineering Research Council of Canada. We thanks Dr. Aya Bamba for her help on analyzing Suzaku data. WWT thanks the Natural Science Foundation of China for support. RY was supported in part by a Grant-in-aid from the Ministry of Education, Culture, Sports, Science, and Technology of Japan (No. 21740184). Upon the submission of our manuscript, we became aware of the recent work by Acero et al.(2009) on the HESS J1731-347/SNR G353.6-0.7 system with independent approaches.

## REFERENCES

- Abdo et al. 2009, ApJ, submission, see arXiv:0902.1340  
 Acero, F. et al. 2009, submission, arXiv:0907.0642

- Aharonian, F., Akhperjanian, A.G. et al. 2006, ApJ, 636, 777
- Aharonian, F., Akhperjanian, A.G., Bazer-Bachi, A.R. et al. 2007, A&A, 467, 1075
- Aharonian, F., Akhperjanian, A. G., Barres de Almeida, U. et al. 2008, A&A, 477, 353
- Bamba, A., Yamazaki, R., Ueno, M., Koyama, K. 2003, ApJ, 589, 827
- Bamba, A., Yamazaki, R., Yoshida, T. et al. 2005, ApJ, 793, 802
- Butt, Y.M., Schneider, N., Dame, T.M., Brunt, C. 2008, MNRAS, 385, 1764
- Camilo, F., Ransom, S.M., Gaensler, B.M., Lorimer, D.R., 2009, ApJ. 700L, 34
- Chang, C., Konopelko, A., Cui, W. 2008, ApJ, 682, 1177
- Fang, J., Zhang, L. 2008, MNRAS, 384, 1119
- Katagiri, H., Enomoto, R., Ksenofontov, L.T. et al. 2005, ApJ, 619, 163
- Kargaltsev, O., Pavlov, G.G. 2008, AIPC, 983, 171
- Koyama, K., Tsunemi, H., Dotani, T. et al. 2007, PASJ, 59, 23
- Li, X.Y., Lu, F.J., Li, Z. 2008, ApJ, 682, 1166
- Pretorius, M. L. 2007, A&A, 2007, 461, 1103
- Gaensler, B.M., Slane, P.O. 2006, Ann.Rev.Astr.Ap., 44,17
- Takahashi, T., Abe, K., Endo, M. et al. 2007, PASJ, 59, 35
- Tian, W.W., Leahy, D.A., Haverkorn M., Jiang, B. 2008, ApJ, 679, L85
- Tian, W.W., Li, Z., Leahy, D.A., Wang, Q.D. 2007, ApJ, 657, L25
- Uchiyama, Y., Aharonian, F.A., Takahashi, T. et al. 2007, Nature, 449, 576
- Voges, W., Aschenbach, B., Boller, Th. et al. 1999, A&A, 349, 389
- Yamazaki, R., Kohri, K., Bamba, A. et al. 2006, MNRAS, 371, 1975
- Zuo, Y.X., Yang, J., Shi, S.C. et al. 2004, CHJAA, 4, 390

Table 1. Spectral fit results<sup>a</sup>

Parameter	PS <sup>b</sup>	PS <sup>c</sup>	K1 <sup>b</sup>	K2 <sup>b</sup>	K3 <sup>b</sup>	ER <sup>b</sup>	WR <sup>b</sup>
$\chi^2/d.o.f.$ . . . . .	125/115	218/235	23/24	56/56	44/48	36/24	70/87
$N_{\text{H}}$ ( $10^{22}$ cm <sup>-2</sup> ) . .	$3.18^{+0.23}_{-0.21}$	$2.10^{+0.06}_{-0.06}$	$1.39^{+0.60}_{-0.85}$	$1.28^{+0.23}_{-0.19}$	$0.79^{+0.13}_{-0.15}$	$1.40^{+0.83}_{-0.74}$	$1.44^{+0.50}_{-0.48}$
Photon index . . . . .	$4.70^{+0.22}_{-0.20}$		$1.74^{+0.62}_{-0.22}$	$2.25^{+0.23}_{-0.11}$	$2.13^{+0.23}_{-0.21}$	$3.38^{+1.12}_{-0.90}$	$2.17^{+1.32}_{-0.30}$
Temperature(keV)		$1.19^{+0.05}_{-0.04}$					
Norm ( $10^{-4}$ ) . . . . .	$390^{+120}_{-100}$	$1852^{+116}_{-116}$	$0.7^{+1.0}_{-0.3}$	$5.6^{+1.9}_{-1.4}$	$3.6^{+1.1}_{-0.8}$	$21^{+49}_{-14}$	$17^{+11}_{-6}$
Flux <sup>d</sup> . . . . .	34.9	544	2.6	10.4	7.7	8.5	34.9

Note. — <sup>a</sup> Regions of spectral interest: PS - the bright compact source (the radius of the source is  $\sim 3$  arcmin in Suzaku image larger than that (40 arcsec) in *XMM-Newton* image); K1, K2 and K3 -three bright knots; ER - the eastern half of the ring excluding K2 and K3; WR - the western half of the ring excluding K1; See details in text. Quoted uncertainties are at 90% confidence level. An absorbed power-law model is used to fit all spectra. <sup>b</sup> Spectra obtained from *XMM-Newton*. <sup>c</sup> Spectra obtained from Suzaku. <sup>d</sup>2-10 keV (1-10 keV for Suzaku) intrinsic flux in units of  $10^{-13}$  ergs s<sup>-1</sup> cm<sup>-2</sup> for *XMM-Newton*.

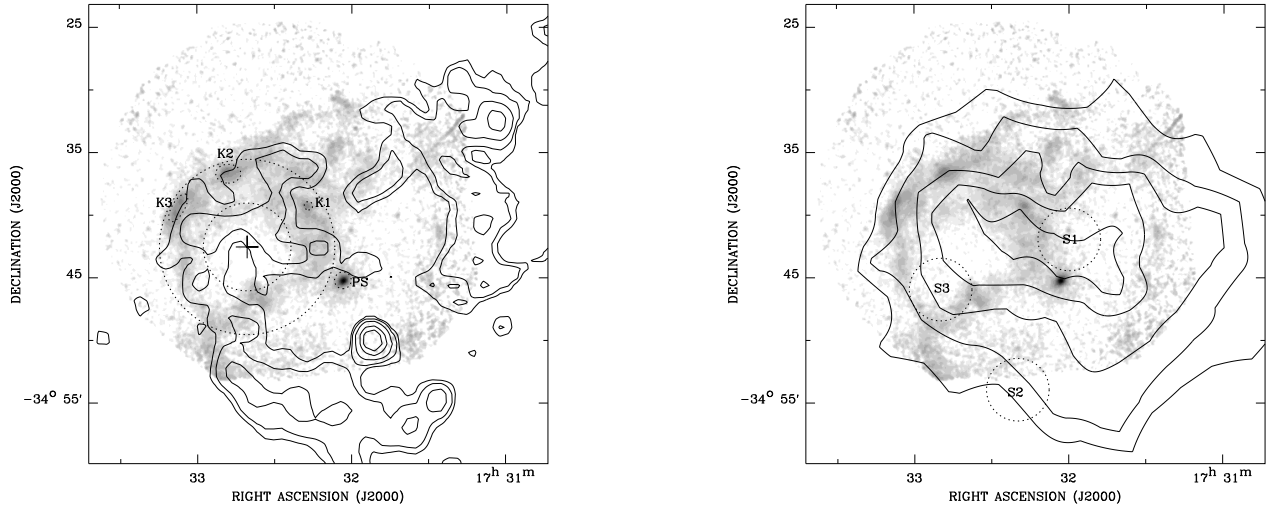


Fig. 1.— Smoothed *XMM-Newton* 0.8-7 keV intensity (greyscale) image overlaid with contours of the VLA radio continuum emission (a) and HESS gamma-ray emission (b), respectively. The greyscale is logarithmically coded between  $(0.5-250) \times 10^{-4}$  cts s<sup>-1</sup>. a: The region enclosed by the two dotted circles outlines the ring-like feature, while the small ellipse /circle outline the bright knots (K1, K2 and K3) and the compact source (PS). b: The circles show the regions where the CO spectra are extracted from.

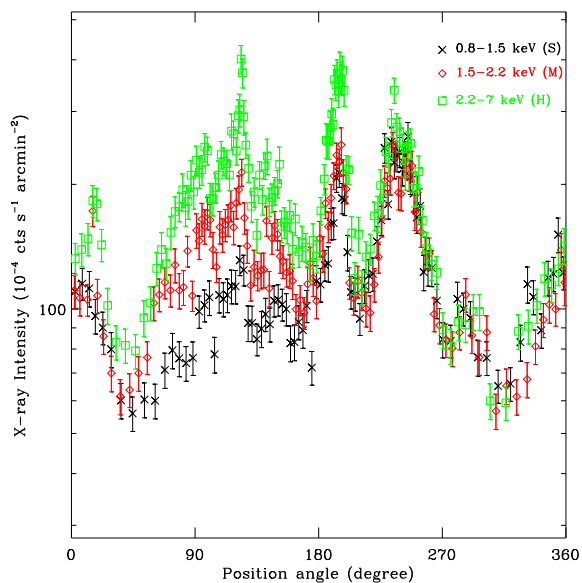


Fig. 2.— Azimuthal X-ray intensity distributions of the ring, extracted from an annulus, with inner-to-outer radii of  $3.5\text{--}7'$ , centering at a position marked by a cross in Fig. 1a. Position angles are measured counterclockwise from south.

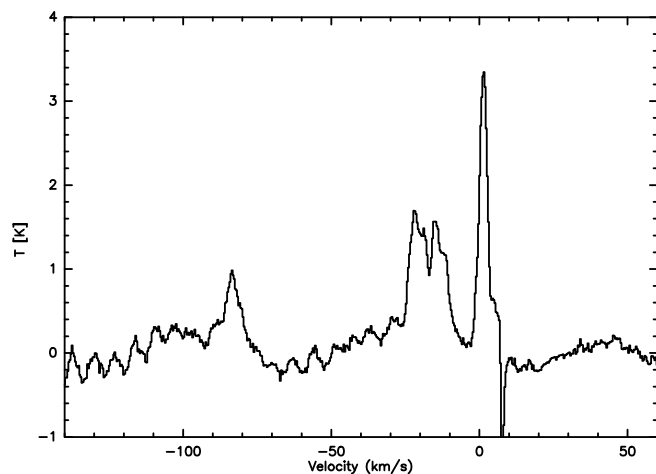


Fig. 3.— The CO spectrum from the TeV source peak (S1)